University of Huddersfield Repository

Harrison, Robert W., Greaves, Graeme, Hinks, J. A. and Donnelly, S. E.

A study of the effect of helium concentration and displacement damage on the microstructure of helium ion irradiated tungsten

Original Citation

Harrison, Robert W., Greaves, Graeme, Hinks, J. A. and Donnelly, S. E. (2017) A study of the effect of helium concentration and displacement damage on the microstructure of helium ion irradiated tungsten. Journal of Nuclear Materials, 495. p. 492. ISSN 0022-3115

This version is available at http://eprints.hud.ac.uk/id/eprint/33076/

http://eprints.hud.ac.uk/

A study of the effect of helium concentration and displacement damage on the microstructure of helium ion irradiated tungsten

R.W. Harrison, G. Greaves, J.A. Hinks and S.E. Donnelly

School of Computing and Engineering, University of Huddersfield, Queensgate, Huddersfield, HD1 3DH, UK

Abstract

Transmission electron microscopy (TEM) with *in situ* He ion irradiation has been used to examine the damage microstructure of W when varying the helium concentration to displacement damage ratio, irradiation temperature and total dose. Irradiations employed 15, 60 or 85 keV He$^+$ ions, at temperatures between 500 and 1000°C up to doses of ~3.0 DPA. Once nucleated and grown to an observable size in the TEM, bubble diameter as a function of irradiation dose did not measurably increase at irradiation temperatures of 500°C between 1.0 and 3.0 DPA; this is attributed to the low mobility of vacancies and He/vacancy complexes at these temperatures. Bubble diameter increased slightly for irradiation temperatures of 750°C and rapidly increased when irradiated at 1000°C. Dislocation loops were observed for at irradiation temperature of 500 and 750°C and no loops were observed at 1000°C. Burgers vectors of the dislocations were determined to be $b = \pm 1/2 <111>$ type only and both vacancy and interstitial loops were observed. The proportion of interstitial loops increased with He-appm/DPA ratio and this is attributed to the concomitant increase in bubble areal density, which reduces the vacancy flux for both the growth of vacancy-type loops and the annihilation of interstitial clusters.

Keywords: Tungsten, Irradiation, Fusion, Radiation damage, *In situ* TEM

1 Introduction

Tungsten (W) is anticipated to be used as the divertor armour in the International Thermonuclear Experimental Reactor (ITER) and the Demonstration (DEMO) fusion reactors [1]. The divertor armour is a plasma facing component (PFC) and thus will experience high heat fluxes and displacement damage from 14.1 MeV neutrons and He ion bombardment. The energy of α-particles lost from the plasma as a result of D-T reactions will generally be around 100s of eV; although particles with MeV energies have been measured escaping the plasma confinement of the Joint European Torus (JET) reactor [2]. These particles will impact on the W surface resulting in a profile of He implantation and thus also a variation of the ratio of He concentration (He-appm) to damage (displacement per atom (DPA)) with depth.

Recent work has examined the effects of fast and thermal neutron irradiations (He-appm/DPA ratio ~0) of W and some W-Os-Re alloys using the High Flux Isotope Reactor (HFIR, USA) as well as the Japanese Materials Test Reactor (JMTR, Japan) and the test sodium-cooled fast reactor (Joyo, Japan) [3]–[7]. Hasegawa *et al*. [4],[5] found that, under both thermal and fast neutron spectra at low DPA (<1.0 DPA) and low temperature (<750°C), the damage microstructure of W consists of a mixture of small (<10 nm) dislocation loops and small (<10 nm) voids. At higher temperatures (>750°C) and higher DPA (~1.5 DPA) there is a shift to a damage microstructure that consists solely of voids which are larger in size (~10 nm). Fukuda *et al.* [5] irradiated W and W-Re alloys in HFIR to 1.0 DPA at 500 and 800°C noting that, at the lower irradiation temperature, the damage microstructure consisted

1

of precipitates and dislocation loops around 5–10 nm in diameter. At 800°C the authors observed voids of ~5 nm diameter with no dislocation loops. Tanno *et al.* [6], [7] irradiated W in the Joyo reactor at with fast neutrons at 750°C to 1.5 DPA, noting the formation of a void lattice. A void lattice has also been reported by Sikka and Moeteff [8] who exposed W to a fluence of ~10^{22} n.cm^{-2} in the Experimental Breeder Reactor (EBR-II, USA) at 550°C.

He *et al.* [9] compared the different effects of neutron and proton irradiation on the defect structures in W. The neutron irradiations were performed in JMTR at 600°C to 0.15 DPA and the authors noted larger loops of ~16 nm in diameter than previous neutron studies and smaller voids of around 3 nm in diameter. Yi *et al.* [10], [11] self-ion irradiated w with 2 MeV W$^+$ to a total of 3 DPA at temperatures between 300 and 750°C. At all irradiation temperatures the authors reported that the defect microstructure consisted of loops with no voids, unlike that found in neutron irradiated tungsten. Also observed were small dislocation loops with equal populations of vacancy and interstitial types mainly with $b = \pm 1/2<111>$ but a minority with $b = <100>$. Harrison et al. [12] irradiated W with 15 and 60 keV He$^+$ ions (He-appm/DPA ratios of 40,000 and 2,000 respectively) to doses of 3.0 DPA at temperature of 500, 750 and 1000°C. The authors noted the presence of dislocation loops with $b = \pm 1/2<111>$ and none with $b = <100>$ which was attributed to the presence of He inhibiting $\pm 1/2<111>$ loop mobility as it is theorised that the $<100>$ loop arises from interaction of $b = \pm 1/2<111>$ in body-centred-cubic (BCC) materials. Iwakiri et al. [13] studied the effect of 8 keV He ion irradiation of W using the in-situ technique at room temperature, 600 and 800°C to doses up to 8.0×10^{17} ions.cm^{-2}. The authors noted the presence of helium bubbles that increased from around 2-3 nm in diameter at room temperature to around 20 nm at 800°C attributed to the increase in temperature increasing defect mobility. The authors also observed small defect clusters at room temperature around 2-3 nm in diameter at room temperature. At irradiation temperatures of 600 and 800°C these loops were larger at around 5-10 nm in diameter and formed tangled networks, the authors assume these are interstitial type loops but no detailed analysis has been performed on their Burgers vector or nature (i.e. vacancy or interstitial). El-Atwani et al. [14], [15] studied the response of ultra-fine and nanosize grain W under 2 keV He ion irradiations at 1000°C to doses ~10^{16} ions.cm^{-2}. The authors noted larger bubbles (up to ~10 nm in diameter) formed on the grain boundaries as these provided a large sink for mobile point defects and helium. The authors also noted the presence of bubbles combined with dislocation loops or over pressurised bubble which gave diffraction contrast around the bubble.

Given the variation of He-appm/DPA across the bulk of the divertor (~0 He-appm/DPA) to the surface (>1000s He-appm/DPA), it is critical to know how the resulting damage microstructure of W varies over this range. Previous studies are difficult to compare with one another due to the differing irradiation conditions (i.e. projectile, irradiation temperature, starting material and fluence/dose). The current work builds on our previous preliminary results [12] whereby we perform experiments at different temperatures, He ion beam energy (to achieve different He-appm/DPA ratios) and by observing *in situ* as the He fluence (and thus damage dose) increases. Simply by increasing the energy of the He ions, the amount of implanted helium is reduced as an increased percentage of the ions are transmitted through the TEM foil at higher energies. Thus, it has been possible to generate a self-consistent data set that charts the effects of varying these three parameters on the microstructural defects of He ion irradiated W.

2 Experimental

TEM foils of W were prepared from commercially available foil (Alfa-Aesar, 99.95 wt.%, main impurity C 0.003 wt.%) by electropolishing. The *Stopping Range of Ions in Matter* (SRIM-2013) Monte Carlo code [16] was used to calculate DPA and helium concentration from implantation, using

the method of DPA calculation proposed by Stoller *et al.* [17]. Further details of sample preparation and SRIM calculations can be found in our previous work [12]. *In situ* ion irradiation was performed at the Microscopes and Ion Accelerators for Materials Investigation facility (using the MIAMI-1 system) described elsewhere [18]. The samples were heated using a Gatan 652 double-tilt heating holder. Post characterisation of the irradiated TEM foils were also made on a JEM-3010 operated at 300 kV. Thickness measurements were made on a range of areas typical of those observed *in situ* so that quantitative comparisons of areal densities of defects could be made. Thickness measurements were performed using electron energy loss spectroscopy (EELS using a Gatan Model 666 parallel detection electron spectrometer) and also by tilting a feature running perpendicular through the TEM foil (such as a grain boundary) about a known angle and measuring its elongation when tilted. Regions analysed found to be around 0.40 λ (where λ is the average free mean path for electrons) corresponding to a thickness of 50–70 nm which was confirmed by the tilting measurements.

Samples were irradiated using 15, 60 or 85 keV He$^+$ ions. Table 1 shows the corresponding He-appm/DPA ratios achieved for the He ion energies used. The ranges of 15, 60 and 85 keV He ions in tungsten are 40, 100 and 150 nm, respectively. However, in a 50–70 nm thick TEM foil the amount of transmitted helium will increase as the He ion energy increases thus decreasing the amount of implanted helium. The amount of damage the ion imparts as it passes through the foil also reduces with increasing energy. However, this drop-off in damage rate is much lower than the concomitant decrease in helium implantation. For example, the vacancies per ion produced in 60 and 85 keV He ion irradiations are 4 and 3, respectively; however, implantation decreases more markedly from 2000 to 500 He-appm per DPA, respectively. The DPA rates of the experiments were ~10^{-3} DPA.s^{-1} and all samples were irradiated to a dose of 3.0 DPA (table 1 shows the fluence needed to achieve 3.0 DPA for each He ion energy) at temperatures of 500 and 750°C or to ~1.3–2 DPA at 1000°C. The samples irradiated with 15 keV He$^+$ ions (He-appm/DPA ratio ~40,000) at 750°C were irradiated to a lower maximum dose of ~2.2 DPA. These lower doses at higher temperatures were necessitated by intergranular fracture and loss of material which rendered experiments to higher doses impossible.

He ion energy/ keV	He-appm/DPA ratio	Fluence at 3.0 DPA /ions.cm^{-2}
15	40,000	1.1x10^{17}
60	2,000	2.4x10^{17}
85	500	3.2x10^{17}

Table 1. Table showing the He ion energy with the corresponding He-appm/DPA ratio and fluence needed to achieve 3.0 DPA

Helium bubble diameters were measured by plotting the intensity profile of a plot along a bubble imaged in underfocus conditions and the distance measured between two minimums on the intensity plot (i.e. the background). Helium bubble diameters were measured using ImageJ [19] with averages calculated based on sample sizes of 30 bubbles each and the errors as the standard deviations. Helium bubble areal number densities (hereon in referred to simply as bubble density for brevity) were measured directly from TEM images by counting the number of bubbles in five areas (i.e. a total of 150 bubbles per irradiation step); the reported densities are given as the averages of the areas and the errors as the standard deviations.

Burgers vectors of the dislocation loops were determined using ***g.b=0*** criterion using ***g*** vectors in the [001] and [113] zone axes. Loop nature analysis was performed using the inside-outside contrast method [20], [21] on 20 to 30 loops in areas of approximately 500 by 500 nm within three different grains per sample, the loops analysed were at least 5 nm in size. The frequency is reported as the average of these three regions and the error as the standard deviation. In order to compare loops sizes

between experiments, only loops with equivalent Burgers vectors imaged under the same two-beam diffraction conditions were considered in order to ensure the consistency and validity of the comparison. Dislocation-loop sizes was measured as the major diameter of the core as observed in projection and only loops of the same Burgers vector imaged under the same diffraction conditions were compared. Areal dislocation loop densities were measured by overlaying images of the same regions taken under different two-beam diffraction conditions in order to include all loops present in the grain whilst also avoiding double counting.

3 Results and Discussion

3.1 General damage microstructure

Figure 1 shows a general overview of the damage features observed in a W sample irradiated with a He-appm/DPA ratio of ~500 as a function of dose (DPA) and temperature. A mixture of small (<1.5 nm) bubbles, which formed an ordered array (bubble lattice) and small dislocation loops (~2 nm) were found at temperatures of 500°C. At higher irradiation temperatures, the bubble size increased with a concomitant decrease in bubble density. Dislocation loops were also observed at irradiation temperatures of 750°C. However at higher irradiation temperatures, the density of these loops decreased and none were observed to form under irradiation at 1000°C agreeing with previous results on the annealing of self-ion irradiated W [22].

3.2. Helium bubble characterisation

3.2.1 The effects of temperature

Helium bubbles were observed at all the irradiation temperatures studied. Micrographs in Figure 2a–c show the bubble size and distribution as a function of temperature (500–1000°C) in samples irradiated with 60 keV He$^+$ ions to a He-appm/DPA ratio of ~2000. Figure 3a–c show plots of bubble size frequency for the He-appm/DPA ratios studied. It can be seen from the histograms in Figure 3a–c that there is a shift from bubble sizes limited to <2.5 nm at 500°C, increasing to a peak frequency at 2.5–3 nm at 750°C to a broader distribution of bubble sizes at 1000°C with a range of 2.5–11.5 nm. Figure 4 shows that bubble density decreased as a function of irradiation temperature for all the He-appm/DPA ratios studied. The mobility of defects in neutron and ion irradiated W has been the subject of many studies aimed at explaining the electrical resistivity recovery mechanisms [3], [7], [22]–[25]. The first stage (stage I) of recovery is attributed to the diffusion of free interstitials which is expected to occur below –173°C [22]. Above –173°C, interstitials are expected to be able to escape from traps and annihilate at sinks (e.g. immobile vacancies, grain boundaries or surfaces) and this is referred to as stage II [22]. Stage III is attributed to monovacancy migration in W and occurs at ~350°C, with an activation energy of 1.7 eV [22], [26]. Stage IV occurs at temperatures above ~720°C and has been attributed to the migration of di-vacancies or vacancy-impurity complexes. Stage V (~870°C) is attributed to the migration of larger vacancy clusters [22]. Thus as the irradiation temperature is increased, the mobility of vacancies increases leading to larger bubbles with a lower bubble density. Bubble coalescence was also observed *in situ* at the irradiation temperature of 1000°C which leads to an even larger average bubble size and lower bubble density than that driven by the increased monovacancy, di-vacancy and vacancy-impurity migration.

Iwakiri et al. [13] performed 8 keV He ion irradiation of W using the in-situ technique at room temperature, 600 and 800°C to doses up to 8.0×10^{17} ions.cm^{-2}. The authors observed bubbles with diameters of around 2-3 nm at room temperature, ~10 nm at 600°C and ~20 nm at 800°C, the increase in bubble size is attributed to the increase in temperature. The closest match with our experimental

conditions is the 15 keV He ion irradiations (He-appm/DPA ratio ~40,000) up to fluences ~10^{17} ions.cm^{-2}. The bubble diameters observed in this work were lower than those reported by Iwakiri et al. and are likely due the lower amount of He implantation in this work as higher He energies were used (resulting in lower He implantation at the same fluence). El-Atwani et al. [14] studies the response of ultra-fine and nanosize grain W under 2 keV He ion irradiations at 1000°C to doses ~10^{16} ions.cm^{-2}. The authors noted larger bubbles formed on the grain boundaries as these provided a large sink for mobile point defects and helium. Bubble diameters were between 2-7 nm which is in good agreement with our work with 15 keV He ion irradiations at a temperature of 1000°C up to higher fluences of ~10^{17} ions.cm^{-2} where bubble diameters were between 2.0-10 nm. The larger upper limit of bubble diameters observed in this work may be attributed to the large, micron-sized grained material. This will provide fewer sinks for defect annihilation, meaning the nucleating bubbles will act as the dominant sink, absorbing helium and helium-vacancy complexes leading to growth.

3.2.1 The effects of He-appm/DPA ratio

Figure 5a shows helium bubble diameter as a function of He-appm/DPA ratio. It can be seen that for samples irradiated at 500°C, bubble diameter was similar at ~1.5 nm for all He-appm/DPA ratios. As the irradiation temperature was increased to 750°C, bubble size showed an increase with He-appm/DPA from around 2.0±0.4 nm to 2.3±0.3 nm in diameter which is expected given the increasing amount of helium and higher mobility of vacancies under these conditions. At 1000°C, the bubble diameter increased with increasing He-appm/DPA ratio which is attributed to the higher concentrations of helium and highly mobile vacancies. However, there was not a significant increase in the bubble diameter from 2,000 to 40,000 He-appm/DPA which may be due to limited vacancy supply as higher concentrations of helium will begin to reduce vacancy mobility. From Figure 5b it can be seen that there was an increase in bubble density with increasing He-appm/DPA ratio which is attributed to the higher concentration of He leading to the nucleation of more bubbles.

3.2.3 The effects of dose

At an irradiation temperature of 500°C and for all He-appm/DPA ratios studied, bubbles grew to a size of ~1.5 nm in diameter but did not appear to grow further as a function of dose up to 3.0 DPA. He bubble lattices were observed for all He ion energies at this temperature and the effects of He-appm/DPA ratio on the bubble lattice parameters are discussed in our previous work [27]. The stability of these lattices (in terms of ordering, bubble spacing and bubble diameter) under increasing dose has been reported previously [28]. Figure 6a shows a bubble lattice observed after irradiation of a W sample with a He-appm/DPA of ~40,000 at 500°C to a dose of 1.0 DPA. The results of further irradiation to 2.0 DPA is shown in Figure 6b demonstrating a similar bubble density and size distribution of bubbles. At 750°C, the bubbles grew to ~2.2 nm and then appeared to grow slightly to ~ 2.5 nm with increasing dose, shown in Figure 6c and 6d which were taken at doses of 1.0 and 2.0 DPA, respectively with a concomitant increase in density of bubbles. At 1000°C the effect on the He bubbles of increasing dose was to increase both their size and density. Figure 6e shows a sample irradiated to 1.0 DPA at 1000°C with a He-appm/DPA ratio of 40,000. In Figure 6f it can be seen that the density and size of bubbles had increased as the dose was increased to 2.0 DPA.

Bubble size as a function of dose for all He-appm/DPA ratios and temperatures are shown in Figure 7a–c for He-appm/DPA ratios of 40,000, 2000 and 500, respectively. Bubble diameter was not observed to increase for irradiation temperatures of 500°C and a small increase was observed at 750°C which may have been due to the irradiation temperatures being just at or below the stage IV recovery step in W where vacancy-impurity or di-vacancies become mobile. Bubble diameter

increased with dose for all samples at 1000°C as at this temperature the stage IV (mobility of vacancy-impurity complexes) and stage V (mobility of large vacancy clusters) are activated. The plot in Figure 8a shows areal bubble density as a function of dose for samples with a He-appm/DPA ratio of 40,000 at temperatures between 500 and 1000°C. At the irradiation temperature of 500°C, it can be seen that the bubble density remains fairly constant as a function of dose (between 0.5 and 3.0 DPA) agreeing well with the micrographs in Figure 6a and b. At 750°C the bubble size increased slightly as a function of dose as shown in Figure 7a and density also increased as a function of dose as shown in the micrographs in Figure 6c–d and the plot of bubble density in Figure 8a. At 1000°C the effect of increasing dose was a dramatic increase in both the average bubble size and the average bubble density. This trend of increasing dose with increasing bubble density at 750 and 1000°C was seen for all He-appm/DPA ratios as shown in Figure 8b–c.

3.3 Dislocation loop characterisation

Dislocation loops was observed at irradiation temperatures below 1000°C and were characterised as $b = \pm\frac{1}{2}<111>$ type with no <100> type observed at the lowest He-appm/DPA ratio of 500. This continues the observation made in our preliminary work [12] where no <100> type loops were observed in samples irradiated to He-appm/DPA ratios of 40,000 and 2,000. However, it is still in contrast to previous work on self-ion irradiation reported in the literature [29] where a mixtures of $b = \pm\frac{1}{2}<111>$ and <100> loops are observed . Figure 9 shows an example of Burgers vector analysis for a sample irradiated at 750°C using 15 keV He$^+$ ions to 3.0 DPA imaged close to the $z = [001]$ zone axis. It can be seen that the circled dislocation loops are visible in Figure 9a–d where $g = 110, \bar{1}10, 200$ and $\bar{2}00$, respectively, and that they are invisible in Figure 9e–f where $g = 1\bar{1}0$ and $\bar{1}10$, respectively, which is consistent with a b vector of $\pm\frac{1}{2}[111]$. The loops marked with squares were characterised as $b = \pm\frac{1}{2}[1\bar{1}1]$ as they showed contrast when $g = 200, \bar{2}00, 1\bar{1}0, \bar{1}10$ and $\bar{2}1\bar{1}$ and showed no contrast when $g = \bar{1}\bar{1}0$ and 110 when imaged close to $z = [\bar{1}\bar{1}3]$. This microstructure, dominated by $b = \pm\frac{1}{2}<111>$ loops, is attributed to the presence of He and has been observed previously with FeCr alloys [30] in which <100> loops are formed by the interaction and coalescence of $\pm\frac{1}{2}<111>$ loops. However, in the presence of He, the mobility of the <111> type loops is low leading to less chance of interaction and coalescence with another <111> type loop. At 1000°C, no dislocations were observed which is attributed as this irradiation temperature is above the stage V recovery step, where both interstitial and interstitial cluster mobility are very high and vacancies can thermally dissociate from clusters [31]. The loop nature (i.e. vacancy or interstitial) was characterised using the inside-outside method; an example of the procedure is shown in Figure 9. The loops in the solid circles were characterised as $b = \pm\frac{1}{2}[111]$ using the $g.b = 0$ criterion. It can be seen that these loops show outside contrast in Figure 9b and d when $g = \bar{1}\bar{1}0$ and $\bar{2}00$, respectively, with $s_g > 0$ leading to the loop inclination being determined to be $b = -\frac{1}{2}[111]$ (for outside contrast, $(g.b)s_g > 0$). As $z = [001]$, $b.z < 0$ thus these loop are interstitial in nature [20], [21], [32]. Dashed circles in Figure 9 show vacancy-type loops with $b = \frac{1}{2}[111]$, solid squares indicate interstitial loops with $b = \frac{1}{2}[1\bar{1}1]$ and dashed squares show vacancy loops with $b = \frac{1}{2}[1\bar{1}1]$. The effects of temperature and He-apppm/DPA ratio on the dislocation loop characteristics are discussed below.

3.3.1 The effects of temperature

Figure 10a–c show TEM images of W samples irradiated with a He-appm/DPA ratio of 40,000 at temperatures of 500, 750 and 1000°C, respectively. It can be seen that loops were present in the samples irradiated at 500 and 750°C. However, none were found in the samples irradiated at 1000°C. Ferroni *et al.* [22] examined the effects of high temperatures on self-ion irradiated W noting that for *ex situ* annealing the loop size increased and loop density decreased with no loops observed at 1400°C.

During *in situ* TEM annealing experiments (up to a temperature of 1200°C), Ferroni *et al.* [22] reported an accelerated loss of loops which was attributed to the stage V recovery step which may have been enhanced by the greater surface-to-volume ratio in TEM foils. This is consistent with the current work where no dislocation loops were observed at temperatures of 1000°C. Our work also agrees well with the neutron irradiation results of Hasegawa *et al.* [3] and Fukuda [5] who reported a microstructure that consisted solely of voids and no dislocation loops at 7500 and 800°C respectively.

Figure 11a shows that the frequency of interstitial-type loops increased with temperature with around 60% of loops analysed being interstitial type at 500°C and around 80% of loops being interstitial type at 750°C, as show in the previous example in Figure 9, where around 85% of loops are interstitial type. Also, both interstitial- and vacancy-type loops were observed to be larger at the higher temperature as shown in the histograms in Figure 11b and c for samples irradiated with a He-appm/DPA ratio of ~40,000. In particular, the vacancy loop size showed a dramatic increase during irradiation at 750°C compared to 500°C as shown in Figure 11c. Vacancy loops observed in previous W ion irradiations have been attributed to form directly from cascade collapse [10], [11]. Thus, the mechanism attributed to vacancy loop nucleation under the conditions in this work is in intriguing as they cannot be due to cascade collapse. These vacancy type loops may nucleate from coalescence of vacancy clusters. The dramatic increase in growth of vacancy type looks may be attributed to the increase of vacancy-impurity mobility at higher temperatures where stage IV recovery becomes important (~720°C). The decrease in the fraction of vacancy-type loops with temperature may be due to the increased rate of capture of these mobile vacancies by bubbles. However, from Figure 11c it can be seen that at 500°C the majority (~75%) of vacancy loops are <17.5 nm and at 750°C vacancy loop sizes are predominantly >20 nm. This increase could be due to the higher mobility of vacancies and vacancy clusters leading to coalescence and thus reducing the number density of vacancy-type loops whilst increasing their average size. Figure 11d shows that dislocation density decreases with irradiation temperature for all He-appm/DPA ratios studied here which matches well with the increase in loop size. Loop hopping (stochastic movement of dislocation loops) and coalescence of loops was also observed *in situ* which would lead to a lower density of loops which would be larger in size. Yi *et al.* [11] also noted a rapid decrease in dislocation density as a function of irradiation temperature for self-ion irradiated W and attributed this to the increased mobility of defect clusters driving coalescence at higher temperatures. However, El-Atwani et al. [14], [15] studied the response of ultra-fine and nanosize grain W under 2 keV He ion irradiations at 1000°C to doses ~10^{16} ions.cm^{-2}. The authors also noted the presence of dislocation loops and bubbles combined with dislocation loops or over pressurised bubble which gave diffraction contrast around the bubble. This is contrary to the current work, where no dislocation loops were observed at irradiation temperatures of 1000°C for all He-appm/DPA ratios. It is also contrary to previous works on neutron irradiated W at temperatures above 750°C where the damage microstructure consisted solely of voids [3]–[5] and in-situ annealing experiments of self-ion irradiation work [22] which our work agrees with. The observation of dislocation loops at such high irradiation temperatures by El-Atwani [14], [15] thus appears unusual as defect mobility (interstitials, interstitial clusters and monovacancies) at this temperature will be very high and vacancy clusters will be unstable to thermal dissociation of vacancies [31].

3.3.2 The effects of He-appm/DPA ratio

Figure 12a–c shows TEM images of W samples irradiated at 500°C to 3.0 DPA with He-appm/DPA ratios of 40,000, 2000 and 500, respectively. It can be seen that there was a decrease in loop size with decreasing He-appm/DPA ratio. Figure 13a shows a plot of loop nature frequency against He-appm/DPA ratio revealing that the frequency of interstitial-type loops increased at higher He-appm/DPA ratios. From Figure 7 and 8 it can be seen that the bubble size was similar at around 1.5

nm diameter for all He-appm/DPA ratios. However, the bubble areal number density showed an increase at higher He-appm/DPA ratios. It is expected that the probability of migrating vacancies being trapped by a bubble increased leading to a reduced vacancy flux and thus recombination with interstitials. This would have led to an increase in the relative frequency of interstitial-type loops with increasing He-appm/DPA ratio.

Interstitial loop sizes were similar, at 5–10 nm, for He-appm/DPA ratios of 500 and 2000 but were much larger at 7.5–35 nm for a ratio of 40,000 as shown in Figure 13b. Figure 13c shows a similar trend for vacancy-type loops with sizes of 2.5–10 nm for He-appm/DPA ratios of 500 and 2000 but much larger at 10–30 nm for a ratio of 40,000. The greater size of interstitial loops at a He-appm/DPA ratio of 40,000 can be attributed to the higher density of bubbles at this ratio which would have reduced the flux of vacancies. This would have led to fewer recombination events with migrating interstitials and thus suppressed the growth of interstitial loops. However, this does not account for the larger vacancy loops at this He-appm/DPA value. Although mean damage rate (measured in DPA/s) was kept constant for each He ion energy by controlling the ion beam flux in the experiments, the displacements per ion did vary locally as a necessary consequence of the different ion energies required to achieve the desired He-appm/DPA ratios. This leads to a larger number of displacements locally for a He-appm/DPA of 40,000. From Figure 11c and 12, it can be seen that dislocation areal density is lower for the He-appm/DPA ratio of 40,000 as compared to He-appm/DPA ratios of 2000 and 500. However, the dislocation loops are clearly larger with a He-appm/DPA ratio of 40,000 (Figure 12a) compared with the He-appm/DPA ratios of 2000 and 500 (Figure 12b and c, respectively). The larger number of local displacements per ion for the He-appm/DPA ratio of 40,000 may result in this lower areal density of larger dislocation loops due to the inhomogeneity of damage causing locally-higher concentrations of defects.

The differences in the sizes of interstitial and vacancy loops for a He-appm/DPA ratio of 40,000 (as shown in Figure 13b and c) can be related to the mobility of the point defects. At 500°C, interstitials will be highly mobile resulting in ~80% of loops being >15 nm whereas ~70% of vacancy-type loops were around 5–17.5 nm due to the relatively-lower mobility of vacancies. The loop sizes for both vacancy and interstitial loops observed in the current work match well with previous results by He *et al.* [9] where loops of around 16 nm in diameter were seen in W irradiated in JMTR at 600°C to a dose of ~0.15 DPA. Unfortunately, the nature of the loops was not reported for that study preventing further comparison in this regard.

4 Conclusions

In situ ion irradiation of W has been performed using He ions at 15, 60 or 85 keV achieving He-appm/DPA ratios of 40,000, 2000 and 500, respectively, at irradiation temperatures of 500, 750 and 1000°C up to a maximum dose of ~3 DPA leading to the following conclusions:

1) Helium bubbles were observed for all He-appm/DPA ratios with bubble size increasing with irradiation temperature and areal number density concomitantly decreasing. Vacancies and vacancy-type clusters will be more mobile as the temperature is increased which will lead to bubble growth as well as coalescence of bubbles at higher temperatures.
2) Helium bubble size and areal number density increased with He-appm/DPA ratio. This is attributed to the higher concentration of He leading to the higher nucleation rate and accelerated growth of bubbles.
3) Bubble diameter and areal density as a function of fluence did not appear to increase significantly for irradiation temperatures of 500°C up to the dose studied in this work (3.0 DPA). This is

attributed to the low mobility of small vacancy clusters (di and tri-vacancies) and helium-vacancy complexes at these temperatures below stage IV recovery. At 750 °C a small increase in bubble size and density is observed as the temperature is now above stage IV. At 1000°C, closer to the operating temperature of the divertor in ITER and above both stage IV and V recovery, the bubbles grew in both size and areal number density and this is attributed to increased vacancy cluster mobility.

4) Dislocation loops were observed for all He-appm/DPA ratios at 500°C and 750°C and the loops were characterised as $b = \pm 1/2 <111>$ type with no $b = <100>$ type loops observed. At 1000°C, above the Stage V recovery mechanism, no dislocation loops were observed which is attributed to the high mobility of interstitials, vacancies and larger vacancy clusters at this temperature.

5) Vacancy type dislocation loops were observed for all He-ppm/DPA ratios at 500 and 750°C. Formation of resolvable vacancy type loops is not expected under these conditions as the nucleation mechanism is attributed to cascade collapse. We therefore attribute the nucleation and growth of vacancy type loops in this work to coalescence of vacancy clusters.

6) Dislocation loop populations become more dominated by interstitial type with increased He-appm/DPA ratio. This is attributed to an increase in bubble density with this parameter resulting in a lower flux of vacancies for the growth of vacancy loops and the annihilation of interstitial-type defects.

Acknowledgments

References

[1] H. Bolt, V. Barabash, W. Krauss, J. Linke, R. Neu, S. Suzuki, and N. Yoshida, "Materials for the plasma-facing components of fusion reactors," in *Journal of Nuclear Materials*, 2004, vol. 329–333, no. 1–3 PART A, pp. 66–73.

[2] D. S. Darrow, F. E. Cecil, V. Kiptily, K. Fullard, A. Horton, and A. Murari, "Observation of alpha particle loss from JET plasmas during ion cyclotron resonance frequency heating using a thin foil Faraday cup detector array," *Rev. Sci. Instrum.*, vol. 81, no. 10, p. 10D330, Oct. 2010.

[3] A. Hasegawa, M. Fukuda, S. Nogami, and K. Yabuuchi, "Neutron irradiation effects on tungsten materials," *Fusion Eng. Des.*, vol. 89, pp. 1568–1572, 2014.

[4] A. Hasegawa, M. Fukuda, K. Yabuuchi, and S. Nogami, "Neutron irradiation effects on the microstructural development of tungsten and tungsten alloys," *J. Nucl. Mater.*, 2015.

[5] M. Fukuda, K. Yabuuchi, S. Nogami, A. Hasegawa, and T. Tanaka, "Microstructural development of tungsten and tungsten–rhenium alloys due to neutron irradiation in HFIR," *J. Nucl. Mater.*, vol. 455, pp. 460–463, 2014.

[6] T. Tanno, A. Hasegawa, J.-C. He, M. Fujiwara, S. Nogami, M. Satou, T. Shishido, and K. Abe, "Effects of Transmutation Elements on Neutron Irradiation Hardening of Tungsten," *Mater. Trans.*, vol. 48, no. 9, pp. 2399–2402, 2007.

[7] T. Tanno, a. Hasegawa, J. C. He, M. Fujiwara, M. Satou, S. Nogami, K. Abe, and T. Shishido, "Effects of transmutation elements on the microstructural evolution and electrical resistivity of neutron-irradiated tungsten," *J. Nucl. Mater.*, vol. 386–388, no. 2009, pp. 218–221, 2009.

[8] V. K. Sikka and J. Moteff, "Superlattice of voids in neutron-irradiated tungsten," *J. Appl. Phys.*, vol. 43, no. 12, pp. 4942–4944, 1972.

[9] J. C. He, a. Hasegawa, and K. Abe, "Effects of transmutation elements on the defect structure development of W irradiated by protons and neutrons," *J. Nucl. Mater.*, vol. 377, no. 2008, pp. 348–351, 2008.

[10] X. Yi, M. L. Jenkins, M. Briceno, S. G. Roberts, Z. Zhou, and M. A. Kirk, "In-situ study of self-ion irradiation damage in W and W-5Re at 500°C," *Philos. Mag. A*, vol. 93, no. 14, pp. 1715–1738, 2012.

[11] X. Yi, M. L. Jenkins, K. Hattar, P. D. Edmondson, and S. G. Roberts, "Characterisation of radiation damage in W and W-based alloys from 2 MeV self-ion near-bulk implantations," *Acta Mater.*, vol. 92, pp. 163–177, 2015.

[12] R. W. Harrison, H. Amari, G. Greaves, J. A. Hinks, and S. E. Donnelly, "Effect of He-appm/DPA ratio on the damage microstructure of tungsten," *MRS Adv.*, vol. 1, no. 42, pp. 2893–2899, 2016.

[13] H. Iwakiri, K. Yasunaga, K. Morishita, and N. Yoshida, "Microstructure evolution in tungsten during low-energy helium ion irradiation," *J. Nucl. Mater.*, vol. 283–287, pp. 1134–1138, 2000.

[14] O. El-Atwani, K. Hattar, J. A. Hinks, G. Greaves, S. S. Harilal, and A. Hassanein, "Helium bubble formation in ultrafine and nanocrystalline tungsten under different extreme conditions," *J. Nucl. Mater.*, vol. 458, pp. 216–223, Mar. 2015.

[15] O. El-Atwani, J. A. Hinks, G. Greaves, S. Gonderman, T. Qiu, M. Efe, and J. P. Allain, "In-situ TEM observation of the response of ultrafine- and nanocrystalline-grained tungsten to extreme irradiation environments.," *Sci. Rep.*, vol. 4, p. 4716, 2014.

[16] J. F. Ziegler, "Stopping of energetic light ions in elemental matter," *J. Appl. Phys.*, vol. 85, no. 3, p. 1249, 1999.

[17] R. E. Stoller, M. B. Toloczko, G. S. Was, A. G. Certain, S. Dwaraknath, and F. A. Garner, "On the use of SRIM for computing radiation damage exposure," *Nucl. Instruments Methods Phys. Res. Sect. B Beam Interact. with Mater. Atoms*, vol. 310, pp. 75–80, 2013.

[18] J. A. Hinks, J. A. van den Berg, and S. E. Donnelly, "MIAMI: Microscope and ion accelerator for materials investigations," *J. Vac. Sci. Technol. A Vacuum, Surfaces, Film.*, vol. 29, no. 2, p. 21003, 2011.

[19] C. A. Schneider, W. S. Rasband, and K. W. Eliceiri, "NIH Image to ImageJ: 25 years of image analysis," *Nat Meth*, vol. 9, no. 7, pp. 671–675, Jul. 2012.

[20] D. M. Maher and B. L. Eyre, "Neutron irradiation damage in molybdenum," *Philos. Mag.*, vol. 23, no. 182, pp. 409–438, 1971.

[21] M. L. Jenkins, "Characterisation of radiation-damage microstructures by TEM," *J. Nucl. Mater.*, vol. 216, no. C, pp. 124–156, 1994.

[22] F. Ferroni, X. Yi, K. Arakawa, S. P. Fitzgerald, P. D. Edmondson, and S. G. Roberts, "High temperature annealing of ion irradiated tungsten," *Acta Mater.*, vol. 90, pp. 380–393, 2015.

[23] F. Maury, M. Biget, P. Vajda, A. Lucasson, and P. Lucasson, "Frenkel pair creation and stage I recovery in W crystals irradiated near threshold," *Radiat. Eff. Inc. Plasma Sci. Plasma Technol.*, vol. 38, pp. 1–2, 1978.

[24] R. W. Balluffi, "Vacancy defect mobilities and binding energies obtained from annealing studies," *J. Nucl. Mater.*, vol. 69–70, pp. 240–263, 1978.

[25] D. R. Mason, X. Yi, M. A. Kirk, and S. L. Dudarev, "Elastic trapping of dislocation loops in cascades in ion-irradiated tungsten foils," *J. Phys. Condens. Matter*, vol. 26, no. 37, p. 375701, 2014.

[26] O. El-Atwani, J. A. Hinks, G. Greaves, S. Gonderman, T. Qiu, M. Efe, and J. P. Allain, "In-situ TEM observation of the response of ultrafine- and nanocrystalline-grained tungsten to extreme irradiation environments.," *Sci. Rep.*, vol. 4, p. 4716, 2014.

[27] R. W. Harrison, G. Greaves, J. A. Hinks, and S. E. Donnelly, "Engineering self-organising helium bubble lattices in tungsten," *Sci. Rep.*, vol. 7, p. 7724, 2017.

[28] P. B. Johnson and D. J. Mazey, "Gas-bubble superlattice formation in bcc metals," *J. Nucl. Mater.*, vol. 218, no. 3, pp. 273–288, Mar. 1995.

[29] X. Yi, M. L. Jenkins, K. Hattar, P. D. Edmondson, and S. G. Roberts, "Characterisation of radiation damage in W and W-based alloys from 2 MeV self-ion near-bulk implantations," *Acta Mater.*, vol. 92, pp. 163–177, 2015.

[30] A. Prokhodtseva, B. Décamps, A. Ramar, and R. Schäublin, "Impact of He and Cr on defect accumulation in ion-irradiated ultrahigh-purity Fe(Cr) alloys," *Acta Mater.*, vol. 61, no. 18, pp. 6958–6971, Oct. 2013.

[31] G. S. Was, *Fundamentals of Radiation Materials Science*, 1st ed. New York: Springer-Verlag Berlin Heidelberg, 2007.

[32] H. Föll and M. Wilkens, "A simple method for the analysis of dislocation loops by means of the inside-outside contrast on transmission electron micrographs," *Phys. Status Solidi*, vol. 31, no. 2, pp. 519–524, Oct. 1975.
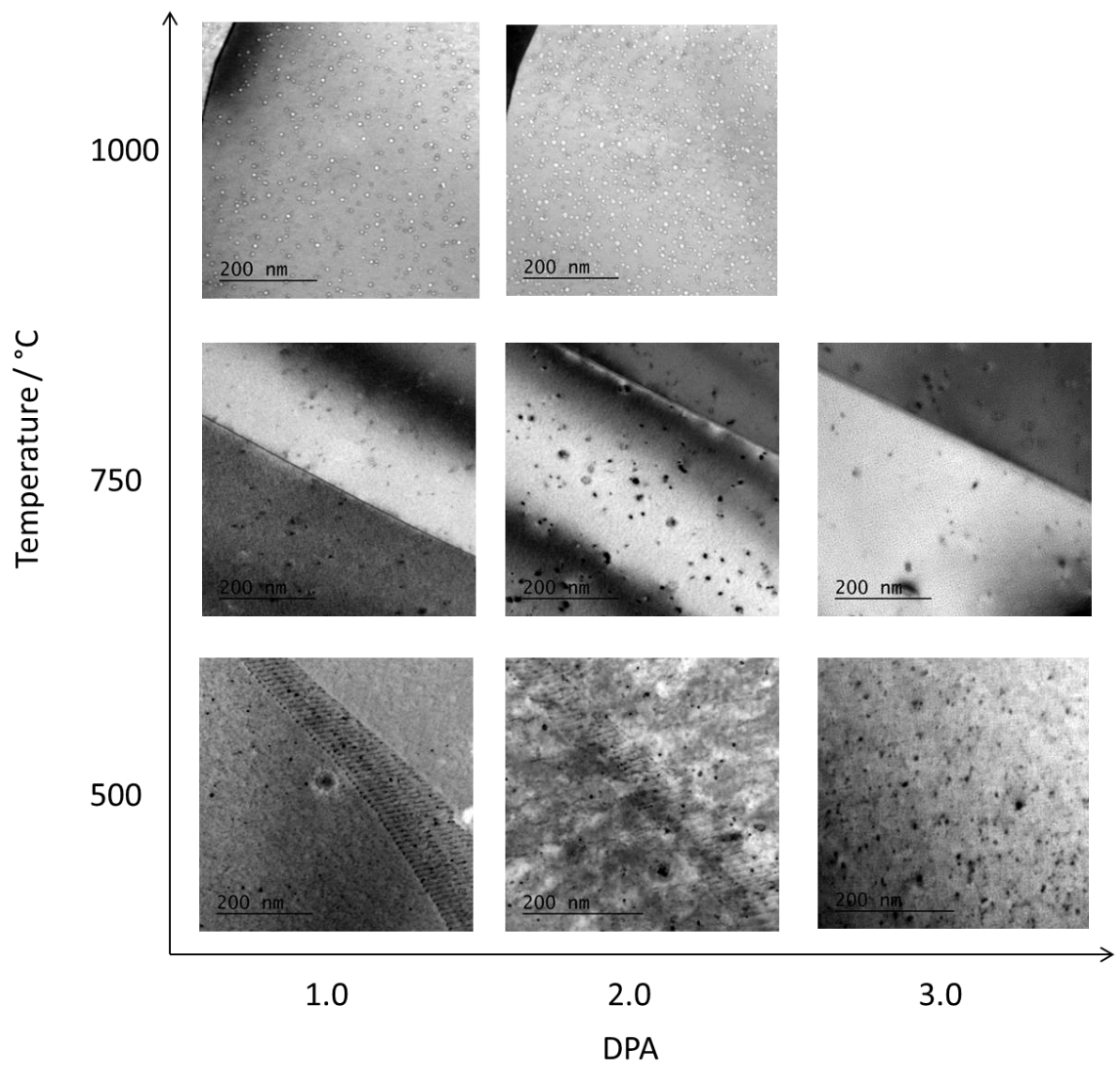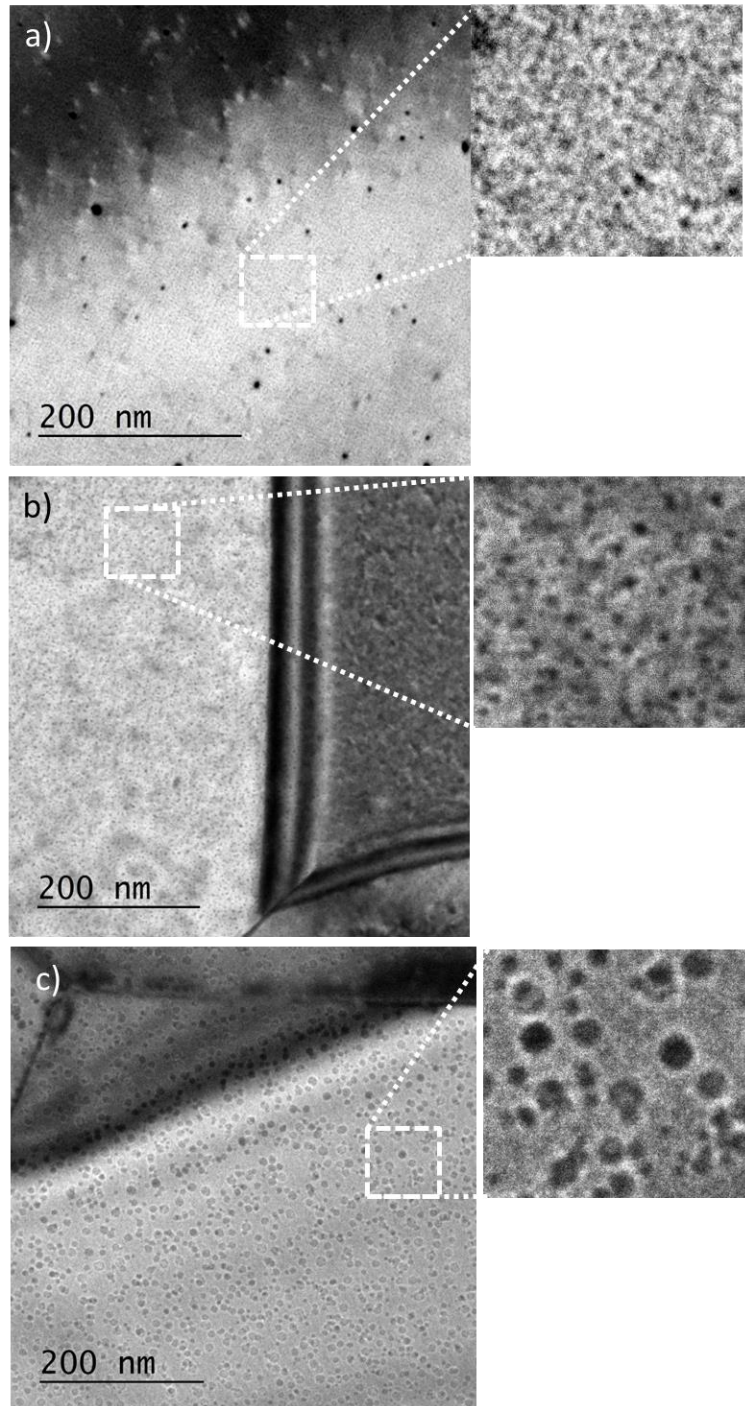
Figure 1. BF-TEM images of W irradiated with 85 keV He$^+$ ions to achieve a He-appm/DPA ratio of 500 showing the damage microstructures as a function of dose (DPA) and temperature. Higher dose, high temperature micrographs are absent due to intergranular fracture and loss of material which rendered experiments to high temperature, high doses impossible.

Figure 2. BF-TEM images of samples irradiated with 60 keV He$^+$ ions to achieve a He-appm/DPA ratio of 2000 to a damage of 1.0 DPA at: a) 500°C with white box highlighting area enlarged to show bubbles of around 2 nm in size; b) 750°C with white box highlighting area enlarged to show bubbles of around 3 nm in diameter; and c) 1000°C with white box highlighting area enlarged to show bubbles with a wide range of sizes from ~2–10 nm in diameter
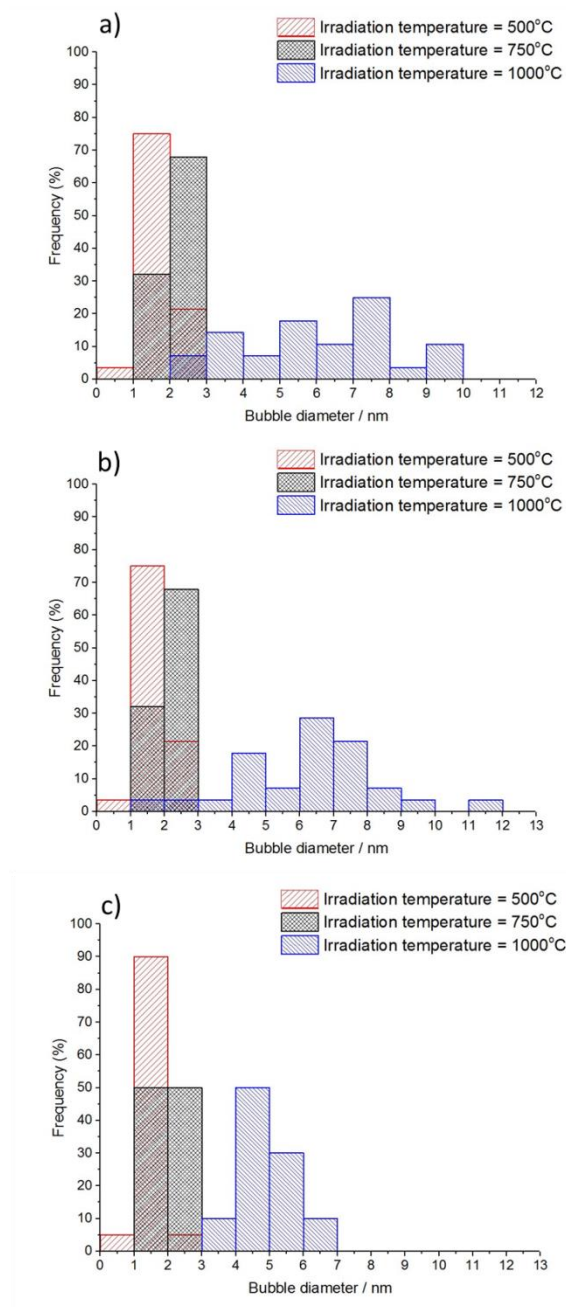
Figure 3. Plots of the frequency of bubble size observed for W samples irradiated at temperatures of 500, 750 and 1000°C to a dose of 1.0 DPA using: a) 15 keV He[+] ions to achieve a He-appm/DPA ratio of 40,000; b) 60 keV He[+] ions to achieve a He-appm/DPA ratio of 2,000; and c) 85 keV He[+] ions to achieve a He-appm/DPA ratio of 500
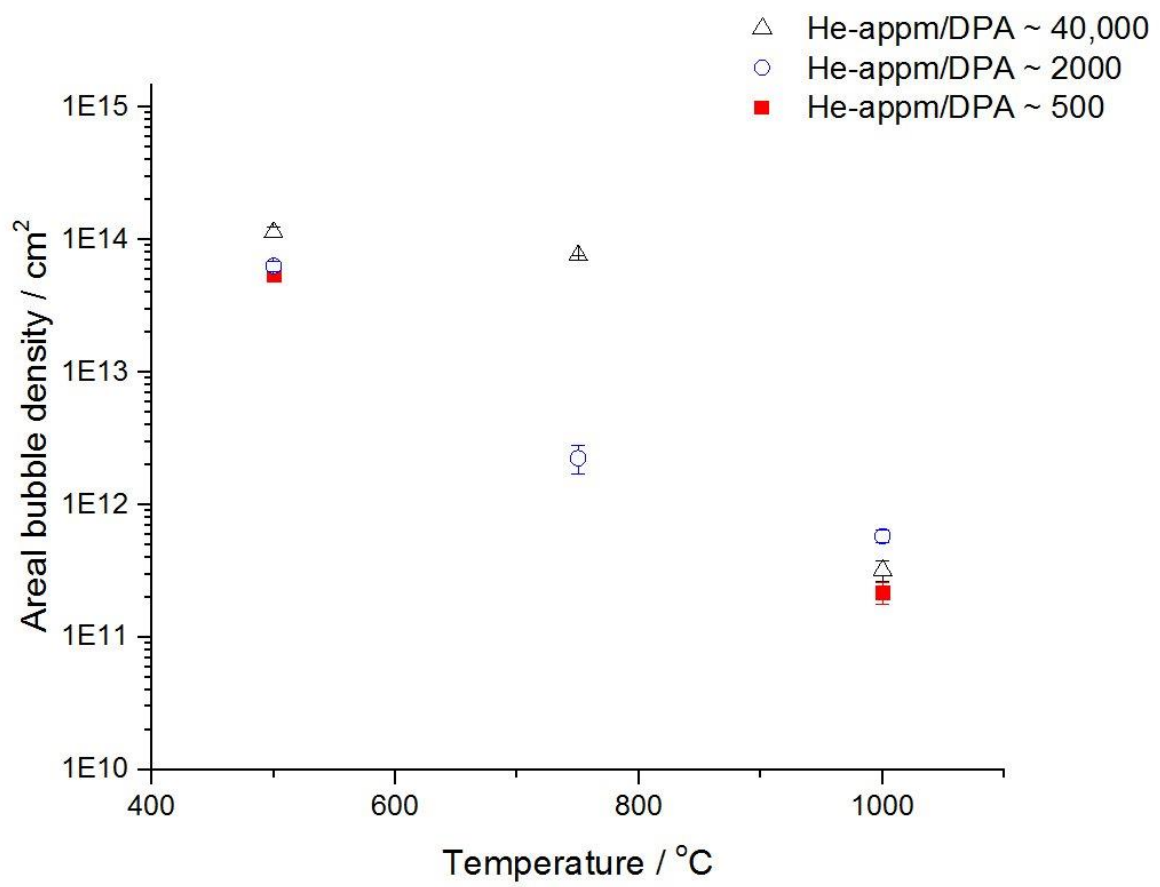
Figure 4. Plot of the helium bubble diameter as a function of temperature for all He-appm/DPA ratios studied at 1.0 DPA
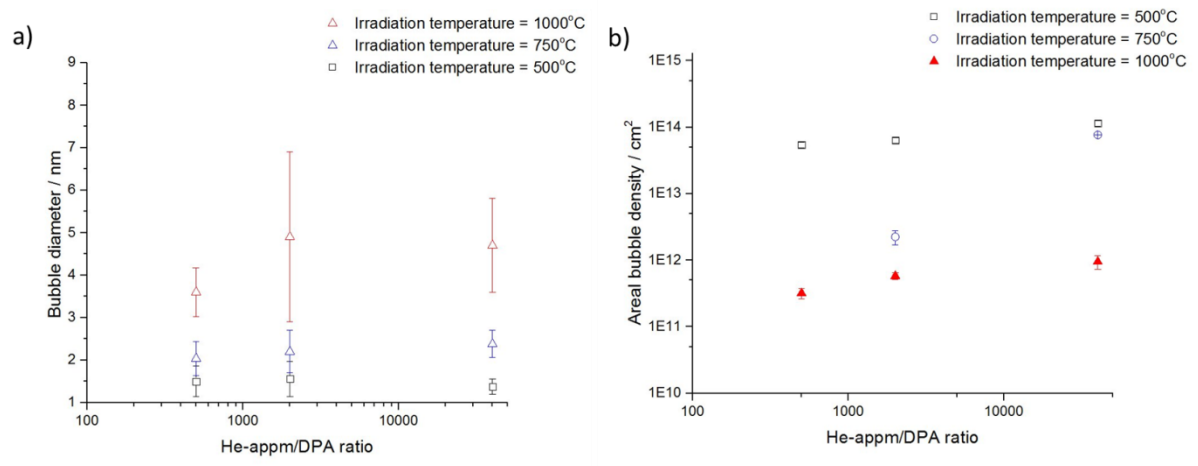
Figure 5. For equivalent damage of 1.0 DPA for all temperatures studied, plots showing as a function of He-appm/DPA ratio: a) helium bubble size; and b) helium bubble areal number density
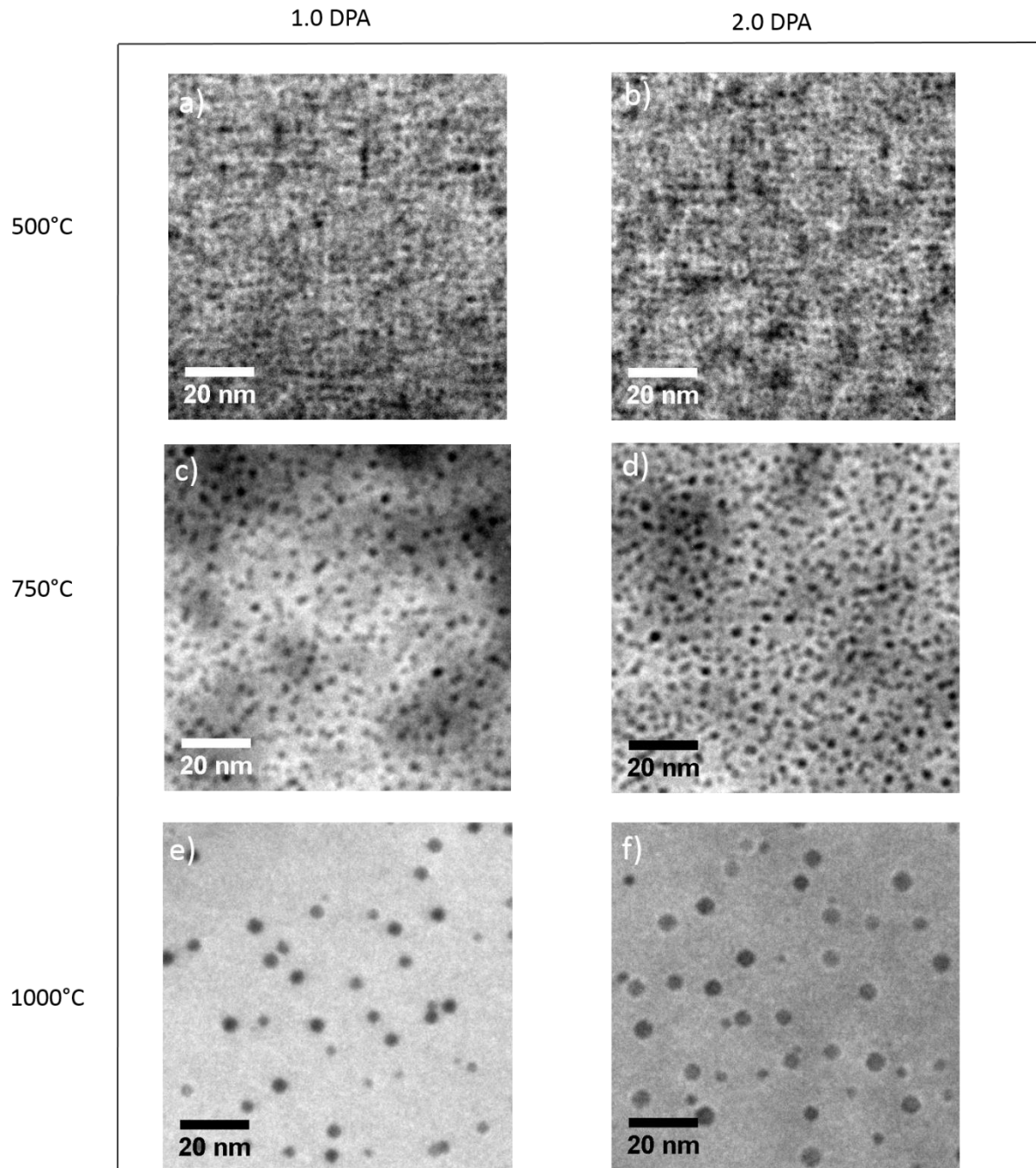
Figure 6. Overfocus BF-TEM images of W sample irradiated with 15 keV He⁺ ions to achieve a He-appm/DPA ratio of 40,000 showing: a) bubble lattice after irradiation to 1.0 DPA at 500°C; b) bubble lattice after irradiation to 2.0 DPA at 500°C demonstrating similar bubble density and sizes compared to 1.0 DPA; c) bubbles after irradiation to 1.0 DPA at 750°C; d) bubbles after irradiation to 2.0 DPA at 750°C demonstrating similar bubble density and sizes compared to 1.0 DPA; e) bubbles after irradiation to 1.0 DPA at 1000°C; and f) bubbles after irradiation to 2.0 DPA at 1000°C demonstrating similar bubble density and sizes compared to 1.0 DPA.
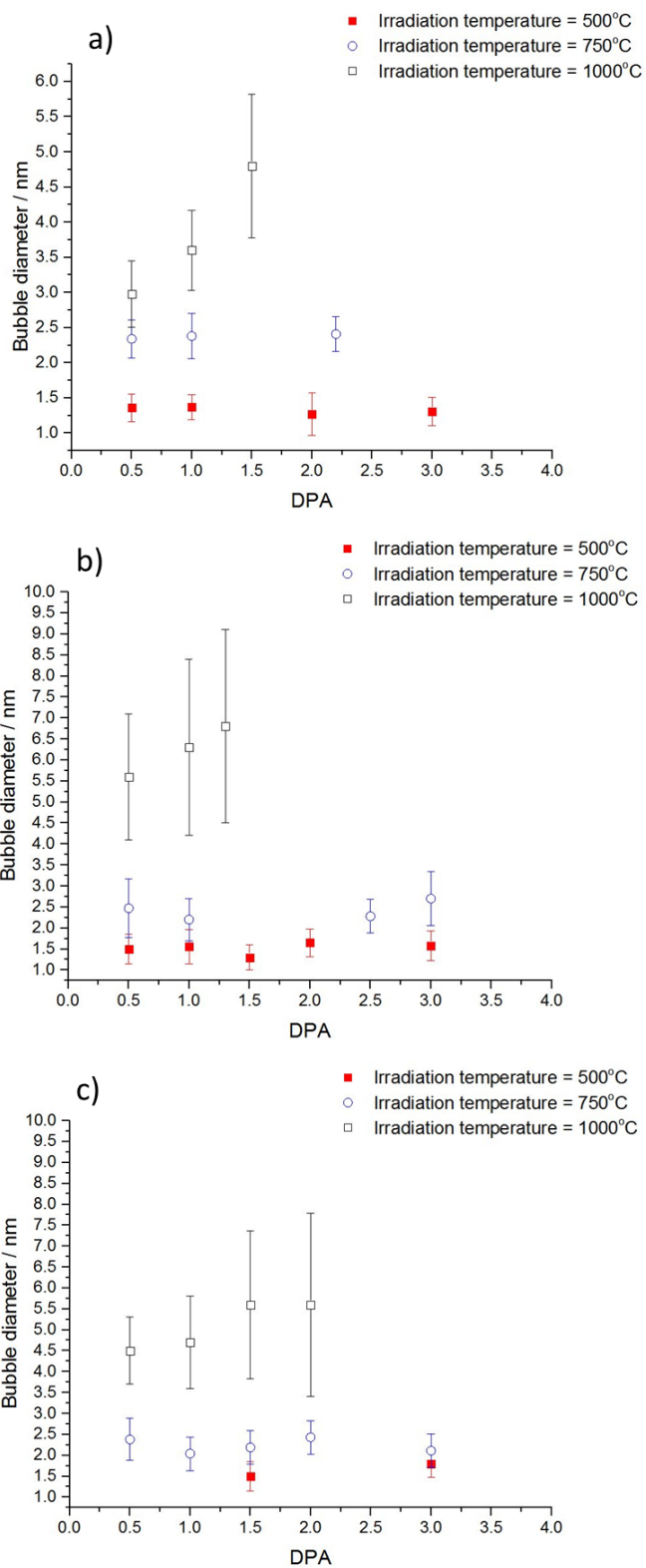
Figure 7. Plots of helium bubble size as a function of damage (DPA) **a)** 15 keV He ions, He-appm/DPA ratio ~40,000, **b)** 60 keV He ions, He-appm/DPA ~2000 and **c)** 85 keV He ions, He-appm/DPA ~500
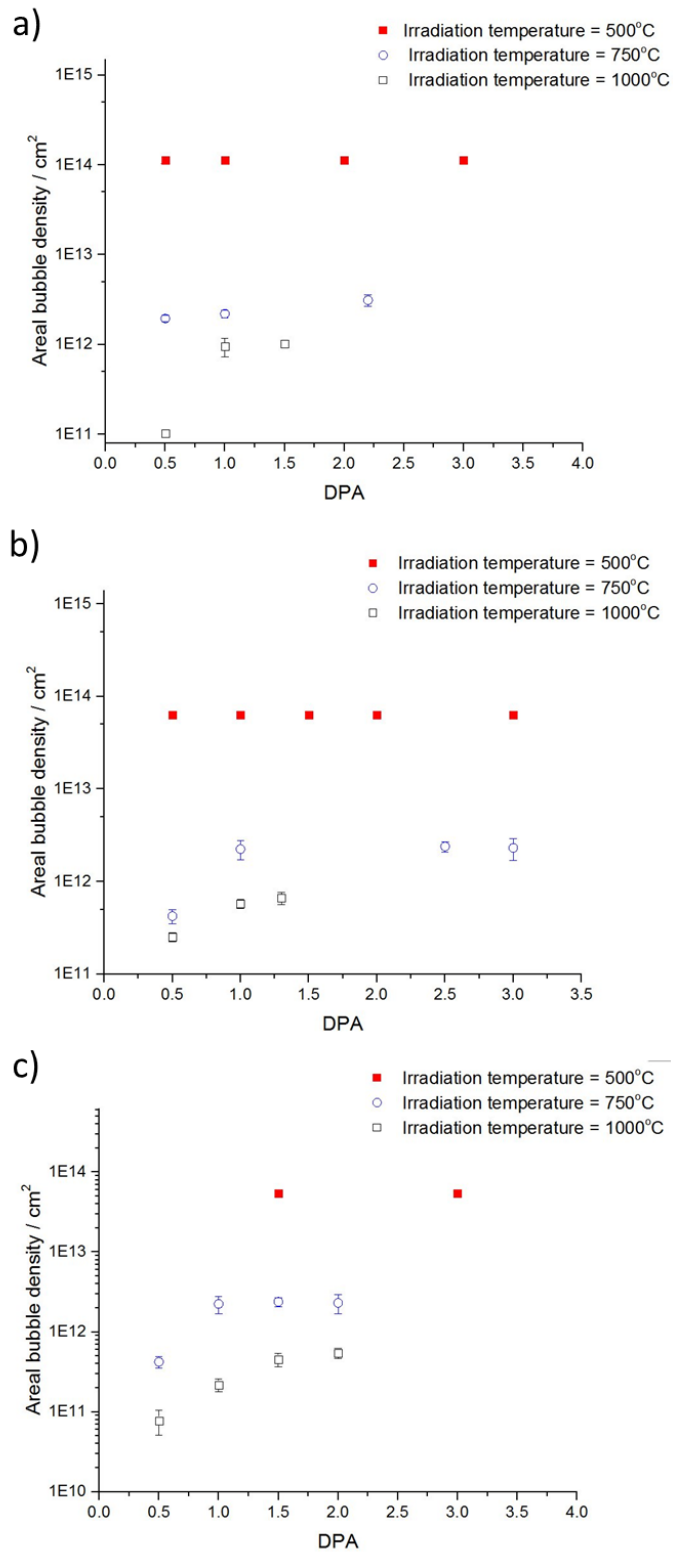
Figure 8. Plots of helium bubble areal density as a function of damage (DPA): a) 15 keV He$^+$ ions achieving a He-appm/DPA ratio of 40,000; b) 60 keV He$^+$ ions achieving a He-appm/DPA of 2000; and c) 85 keV He$^+$ ions achieving a He-appm/DPA of 500
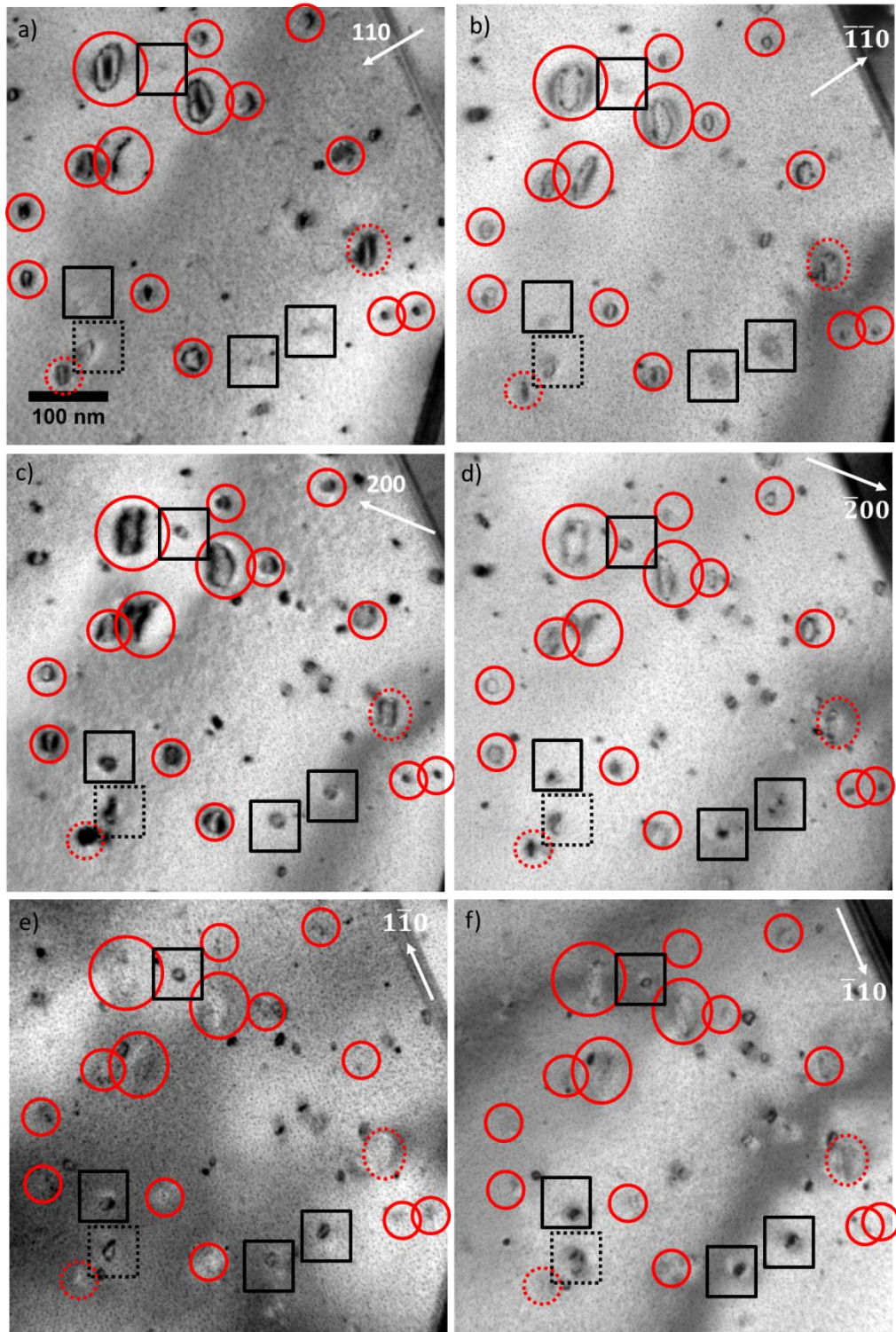
Figure 9. Two-beam TEM images taken close to focus of sample irradiated at 750°C with 15 keV He⁺ ions to achieve a He-appm/DPA ratio of 40,000 to 2.2 DPA: a) $g = 110$; b) $g = \overline{1}10$; c) $g = 200$; d) $g = \overline{2}00$; e) $g = 1\overline{1}0$; and f) $g = \overline{1}10$. Solid circles indicate interstitial loops with $b = \frac{1}{2}[111]$, dashed circles indicate vacancy-type loops with $b = \frac{1}{2}[111]$, solid squares indicate loops with $b = \frac{1}{2}[1\overline{1}1]$ and dashed squares indicate vacancy loops with $b = \frac{1}{2}[1\overline{1}1]$. Scale marker applies to all images.
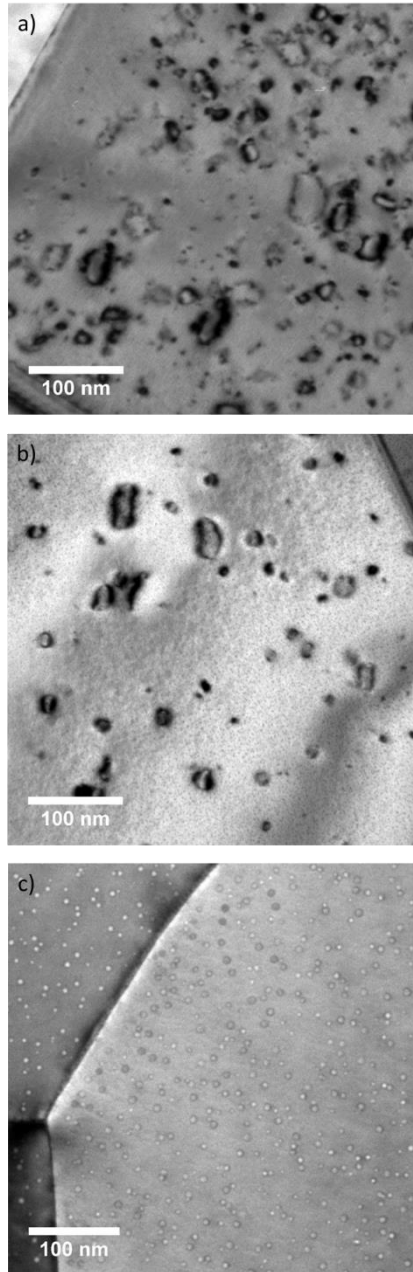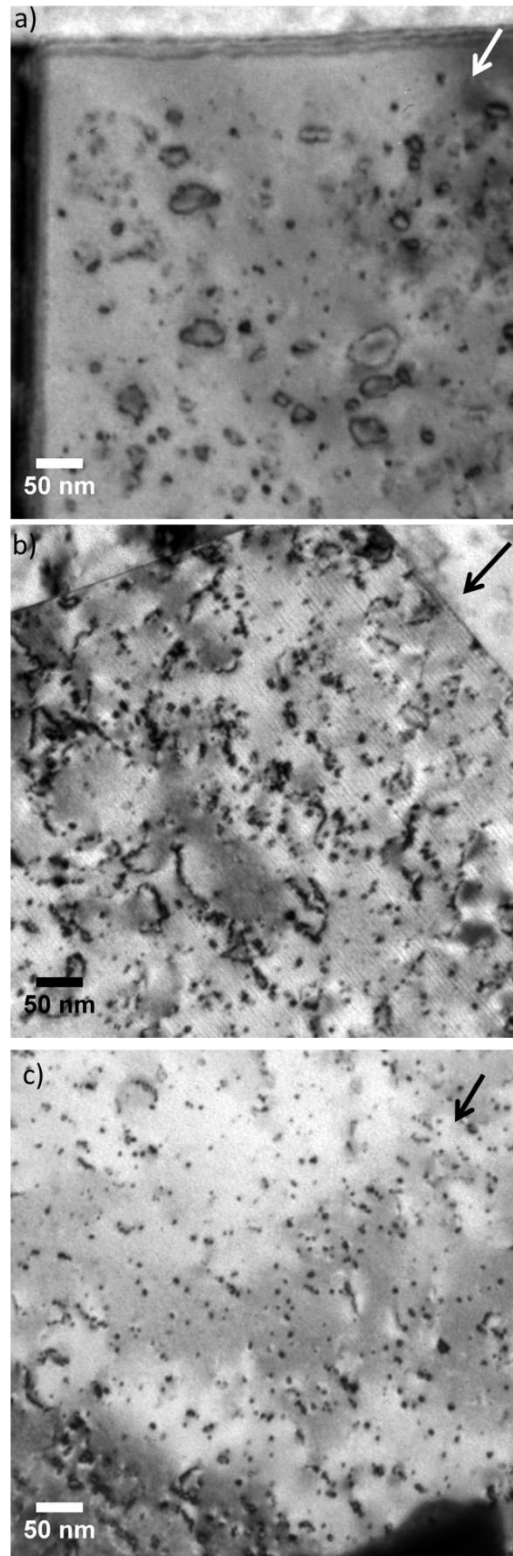
Figure 10. BF-TEM images taken under similar diffraction conditions close to the [001] zone axis of W samples irradiated with 15 keV He$^+$ ions to achieve a He-appm/DPA ratio of 40,000: a) irradiation to 2.2 DPA at 500°C showing a high density of dislocation loops; b) irradiation to 2.2 DPA at 750°C showing a lower density of loops; and c) irradiation to 1.3 DPA at 1000°C showing no loops and the presence of only bubbles.
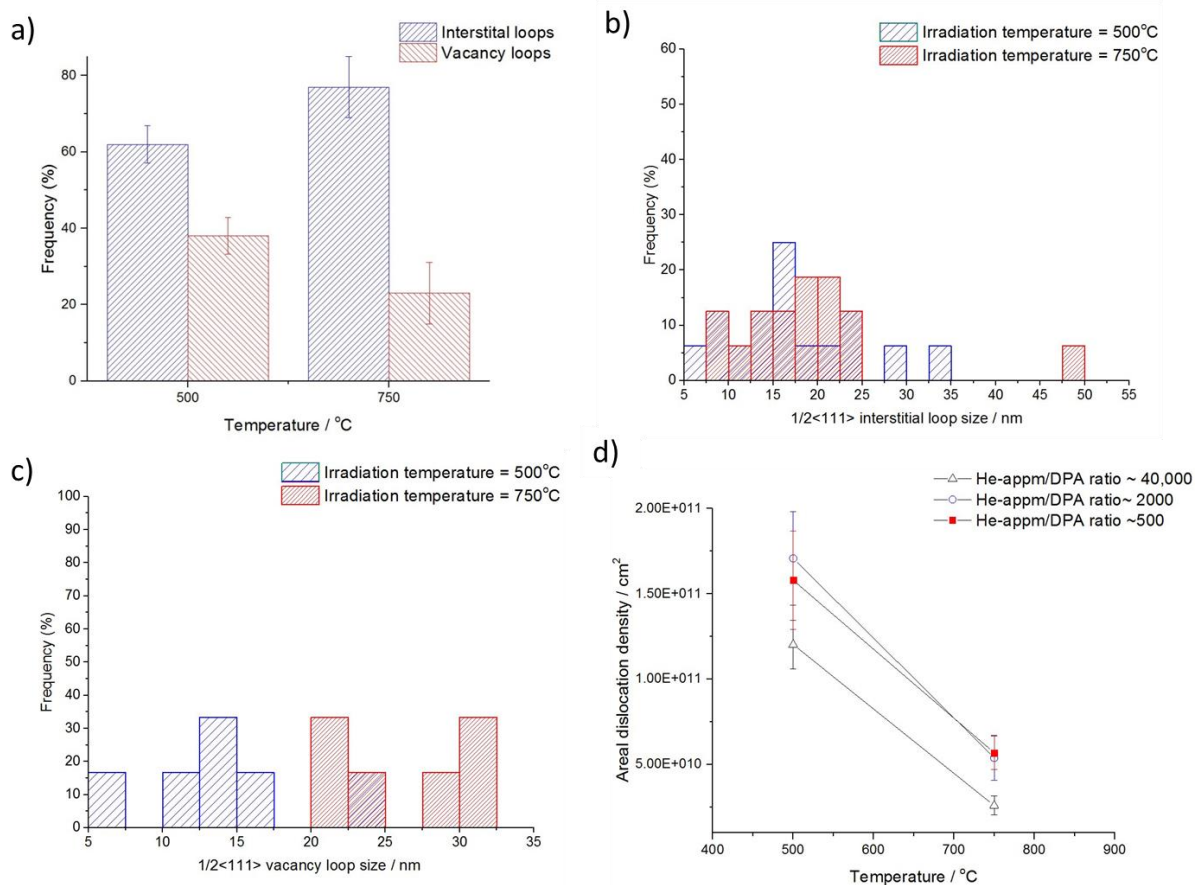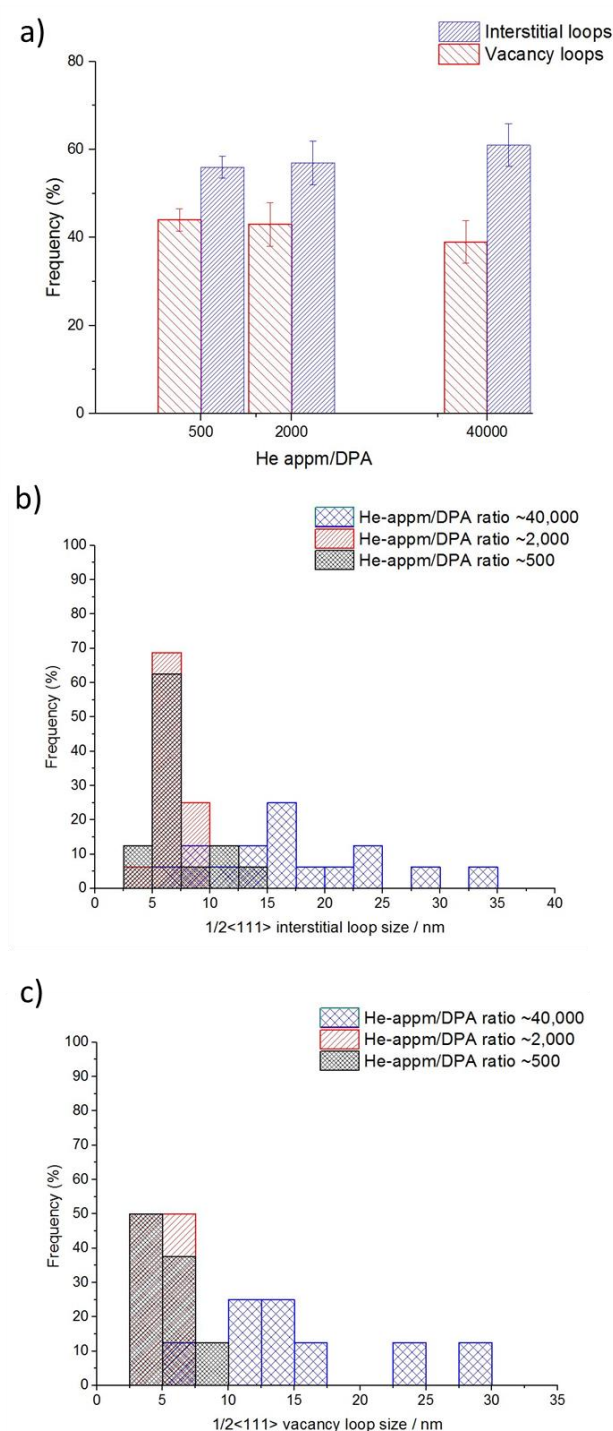
Figure 11. W samples irradiated with 15 keV He$^+$ ions to a He-appm/DPA ratio of 40,000 and dose of 2.2 DPA, plots showing: a) the relative frequency of loop nature demonstrating an increase in the relative interstitial loop population at higher temperatures; b) a histogram of interstitial loop size frequency for ½<111> type loops (imaged close to the [001] zone axis with g = 200 excited) showing an increase in loop size as a function of temperature; and c) a histogram of vacancy loop size frequency for ½<111> type loops (imaged close to the [001] zone axis with g =200 excited) demonstrating an increase in loop size as a function of temperature; d) shows the dislocation areal density (measured from overlaid images taken under several two beam conditions to ensure all loops are counted) for all He-appm/DPA ratios studied demonstrating a decrease in loop density as a function of temperature for all cases

Figure 12. BF-TEM images (taken under similar diffraction conditions close to the [001] zone axis with g =110 (indicated by arrow) excited of W samples irradiated at 500°C with: a) 15 keV He$^+$ ions to achieve a He-appm/DPA ratio 40,000 to a dose of 3.0 DPA; b) 60 keV He$^+$ ions to achieve a He-appm/DPA ratio of 2000 to 3.0 DPA; and c) 85 keV He$^+$ ions to achieve a He-appm/DPA ratio 500 to a dose of 3.0 DPA

Figure 13. Plots showing: a) the relative frequency of loop nature in W samples irradiated at 500°C with 15, 60 or 85 keV He+ ions to achieve He-appm/DPA ratios of 40,000, 2,000 and 500, respectively demonstrating an increase in the interstitial loop population with increasing He-appm/DPA ratio; b) a histogram of interstitial loop size frequency for ½<111> type loops as a function of He-appm/DPA ratio (imaged close to the [001] zone axis with g =200 excited) demonstrating an increase in loop size with He-appm/DPA ratio; and c) a histogram of vacancy loop size frequency for ½<111> type loops as a function of He-appm/DPA ratio (imaged close to the [001] zone axis with g =200 excited) showing an increase in loop size with increasing He-appm/DPA ratio.